Batteries & Supercaps

Research Article
doi.org/10.1002/batt.202400514

Chemistry Europe
European Chemical Societies Publishing

www.batteries-supercaps.org

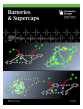

Li Decorated Graphdiyne Nanosheets: A Theoretical Study for an Electrode Material for Nonaqueous Lithium Batteries

M. J. Jiménez,[a] J. Juan,[b] M.S. Sandoval,[a] P. Bechthold,[a] P. V. Jasen,[a] E. A. González,[a] and A. Juan*[a]

In this work, Density Functional Theory (DFT) is used to study pristine and defective GDY. We investigate the effect of Li atom adsorption on the electronic and structural properties of this 2D material. In both cases, the Li atom is located at the corner of the triangular-like pore (H1), but with a slight shift for the defective system. In the perfect system, the Li–C bond distances range from 2.289 Å to 2.461 Å, while in the defective case, they range from 2.237 Å to 3.184 Å. In the perfect case, the GDY–Li system becomes metallic and the Li 2 s states are stabilized. Charge transfer to the surfaces occurs near the vicinity of the Li atom. The C vacancy generates new C=C bonds similar to double bonds, enhancing the interaction with Li through strong conjugation. After Li adsorption, the sum of bond order for all the C atoms increases in both structures, from 0.4 % to 6 %. The Li storage capacity without significant restructuring is six Li atoms. When the atom concentration increases, the OCV values for Li decrease from 0.93 V to 0.23 V. For defective GDY, the specific capacity is 788 $mAhg_{-1}$, which is slightly higher than for pristine case.

1. Introduction

The severe consequences of global warming drive development and the worldwide search for sustainable energy sources that reduce dependence on fossil fuels and the emission of greenhouse gases. Due to the constant improvement of electronic devices, increasingly smaller circuits and significant storage capacities are required to store energy from intermittent or non-intermittent renewable energy sources. For this reason, it is necessary to provide energy for the proper functioning of these devices, so it is extremely important to study the storage/weight and storage/volume relationship to manufacture them, such as for the use of electric vehicles (EVs), portable technology such as personal computers, mobile phones or any electronic device.[1–4]

The study and technological development of portable electronic materials make lithium-ion batteries (LIB) essential due to their high energy density compared to other rechargeable batteries, and they are the ones that best fit these two characteristics.[5] This is why LIBs have become the most popular energy storage devices when compared, for example, to Ni–Cd or Ni–MH batteries.[1] A LIB works by moving lithium ions from the cathode to the anode when charging and the opposite process when discharging.[2]

Anodes in LIBs must have certain requirements. The binding energy of Li atoms should be in the energy window of ~2 eV of the total energy of Li. That is, the average adsorption energy (E_{ads}) of Li on the surface should be larger than the experimental value of the Li cohesion energy, 1.63 eV, and from the Li binding energy, ~3 eV.[2,4,7] If the binding energy is ~1.6 eV, Li segregation can occur, and if it is greater than ~3 eV it cannot function as an anode.[6] In addition, LIBs can be increasingly smaller, lighter, and have minimum charging time and maximum useful life, without neglecting safety. Therefore, the balance of these requirements brings lithium ion technology to the forefront.[2,5,7] However, new materials with high performance are constantly sought.

For batteries, lithium metal anodes are used due to their inherently high specific capacity of 3860 $mAh\,g^{-1}$.[6] But the disadvantage of using alloy-based materials as anodes lies in their drastic variation in volume (greater than 400 %) during the Li insertion/extraction cycles, which leads to a rapid loss of their capacity[2,7] and the Li anode caused safety issues due to dendrite formation.[8]

Materials with low dimensionality are widely studied theoretically and experimentally for their potential applications in catalysis, spintronics, photonics and energy storage, among other applications. Zero-dimensional materials, such as nanoparticles and quantum dots, have emerged as promising candidates for enhancing the performance of lithium-ion batteries due to their high surface area, and fast ion/electron transport. These characteristics enable 0D materials to improve the specific capacity and charge/discharge rates. For instance, carbon quantum dots and silicon nanoparticles have been explored as anode materials, demonstrating enhanced electrochemical performance and reduced degradation over cycling.[9,10] Among the 2D materials, the, C-based materials are

[a] M. J. Jiménez, M.S. Sandoval, P. Bechthold, P. V. Jasen, E. A. González, A. Juan
Instituto de Física del Sur (IFISUR), Departamento de Física, Universidad Nacional del Sur (UNS), CONICET, Av. L. N. Alem 1253, B8000CPB Bahía Blanca, Argentina
+54–291–4595101. Ext: 2818
+54–0291–4595142
E-mail: cajuan@uns.edu.ar

[b] J. Juan
Instituto de Física Aplicada (INFAP), Universidad Nacional de San Luis, CONICET, Ejército de los Andes 950, D5700 HHW San Luis, Argentina

Supporting information for this article is available on the WWW under https://doi.org/10.1002/batt.202400514

constantly studied theoretically and experimentally for their sp^3, sp^2 and sp hybridized states that can give rise to numerous allotropes in nature, such as,[1,11] carbon nanotubes,[12–14] Graphene,[15–18] graphyne,[4] etc. Due to their potential technological applications, new carbon allotropes with specific properties are designed and being attempted to be synthesized, which constitutes a challenge in the field of materials science.

Many of these materials are studied and used commercially for energy storage, particularly as an anode material due to their flat charge, discharge plateau, and excellent cycling stability. However, its maximum capacity is limited.[5] In the case of graphite, it is used as an anode due to its high diffusion of lithium ions (high power) and high stability against Li intercalation (small volume change). Moreover, for a configuration of one Li atom for every six C atoms, the maximum specific capacity is 372 $mAh\,g^{-1}$.[5,6,19,20] The effect of the external biaxial strain on the adsorption and diffusion of Li on the graphyne as an anode material in the LIB was studied by DFT calculations. An increase in Li adsorption energy is predicted with a larger biaxial strain and for the Li_6C_6 configuration, the graphyne capacity reaches 2233 mAh/g, twice as large as without strain.[4] Carbon nanotubes (CNT) have been widely studied for LIBs due to the effective diffusion of lithium ions into stable sites located on the nanotube surface and/or into individual nanotubes through the top layer or side wall openings.[2]

Graphdiyne (GDY) is a 2D carbon allotrope that belongs to the graphyne family (see Figure 1a). GDY is regarded as a highly stable allotrope with good stability at room conditions.[21] The GDY structural model was theoretically proposed in 1997.[12–14,16] Li et al. in 2010 were the first to synthesize GDY with a cross-coupling reaction on the surface of copper.[22] GDY has a network structure composed of sp^2- and sp- hybridized carbon. The sp^2-hybridized C atoms form hexagons which are joined together by two acetylenic linkages (–C≡C–C≡C–).[23–25] The rigid and planar carbon network with different stable chemical bonds between the atoms causes its excellent chemical stability, high electrical conductivity,[22] high carrier mobility (10^{4-5} $cm^2\,V^{-1}\,s^{-1}$),[19] optimal bandgap for semiconductors compared to graphene[26] and tunable electronic properties due to high electron cloud density. The evenly distributed triangular pores, lead to several applications in the fields of catalysis, energy, sensors, electronics, optoelectronics, and the capability to work as ideal 2D gas filters.[19,27] The addition of diacetylenic links result in an increase in pore diameter to 11.38 Å, suggesting possible uses in energy storage.[21] This unique porous structure asymmetrically conjugated p electrons, and semiconducting features of GDY may pave the way for a technological breakthrough in Li ion batteries.[25]

Previous studies with DFT indicated that GDY has a natural band gap between 0.46 and 1.10 eV,[21] which originates from the inhomogeneous p-bindings between differently hybridized carbon atoms in this sp-sp^2 hybridized carbon network.[20,25]

Regarding gas adsorption, previous works show that metals can be stably adsorbed on GDY. In particular, Li has the smallest density and high charge density, and is not easily polarized among all studied metals so far.

In this work, we conducted Density Functional Theory (DFT) work for pristine and defective GDY. We studied the effect of Li atoms doping on the electronic and structural properties of this 2D material. We modeled the structure of the pristine GDY and examined its stability. Moreover, the electronic properties and the possible adsorption sites are studied. The OCV and the specific capacities for an increased atom concentration are calculated. Next, the surface defects (vacancies) are studied and Li is adsorbed on the most stable site. This work uniquely addresses both pristine and defective GDY structures, providing detailed insights into the effects of Li atom adsorption on their electronic and structural properties. The study uncovers that defects in GDY significantly enhance Li interaction through the formation of new C=C bonds, leading to strong conjugation. Additionally, the investigation reveals distinct differences in Li–C bond distances between pristine and defective systems, highlighting the critical role of defects in modulating material properties.

Methodology and Model

Computational Details

The structures were calculated based on density functional theory (DFT). Spin-polarized total energy DFT calculations are carried out using the Vienna Ab-Initio Simulation Package (VASP),[28–30] and the Projector Augmented-Wave (PAW) pseudopotentials[31] are used to reproduce the atomic core effects in the electronic density of the valence electrons by the generalized gradient approximation (GGA). For electron exchange and correlation effects, the Generalized Gradient Approximation due to Perdew, Burke and Ernzerhof is adopted.[32]

The kinetic energy cut-off for the plane wave expansion of the electronic wave function is 600 eV. The energy convergence criterion used is 1 meV. The plane wave basis is generated considering 4 valence electrons for C ($2\,s^2 2p^2$) and 1 valence electron for Li ($2\,s^1 2p^0$). The first Brillouin zone (BZ) integration used is a gamma centered Monkhorst – Pack scheme[33] on well-converged k-point meshes of 11×11×1. Van der Waals (vdW) corrections are included using the Grimme DFT–D3 approach to address dispersion interactions.[34]

The total energy of C and Li isolated atoms is required to calculate adsorption energies, which is done by the calculation with a single atom in a cubic supercell of length 10 Å with only the gamma point of the Brillouin zone. The adsorption energy[35,36] of the Lithium atoms on GDY monolayers is given by:

$$E_{ads} = E(LiSystem) - [E(System) + E(Li)] \quad (1)$$

where $E(Li)$, $E(System)$ and $E(LiSystem)$ are the total energy of a Li atom, the pristine or defective GDY layer before and after adsorption, respectively. Note that negatives and positive values indicate favorable and unfavorable adsorption, respectively.

The concentration of Li is uniformly increased step-wise on favourable sites. To determine the performance of the material as an anode, the values of the average open circuit voltages (OCV) of the charging/discharging process are calculated as:

Research Article
doi.org/10.1002/batt.202400514
Chemistry Europe
European Chemical Societies Publishing

$$OCV = \frac{-E(Li_nDY) + nE(Li) + E(GDY)}{ne} \quad (2)$$

where $E(Li_nGDY)$ and $E(GDY)$ are the total energies of the system with n Li atoms and the GDY system, respectively. $E(Li)$ is the energy of the single Li atom in the crystalline system, and e is the fundamental unit charge.[37,38]

The storage capacity values are calculated according to:[39]

$$C_x = \frac{xF}{3.6\ M_{GDY}} \quad (3)$$

where M_{GDY} is the *GDY* molar mass, x is the number of the absorbed Li atoms on GDY and F is the Faraday constant.[39]

In order to understand the interaction between the adsorbates and the surfaces we explored the electronic properties such as density of states (DOS) and atom-projected density of states (PDOS) of the most stable systems. Bader analysis as implemented by Tang et al. is used to calculate electronic charges on atoms.[40,41]

On-the-fly force field machine learning (MLFF) from ab initio molecular dynamics (AIMD) is applied in order to verify the local stability of the decorated systems. The MLFF procedure consists of first starting on-the-fly training of the structure. Afterwards, a continuation simulation with a refit for fast prediction mode is done to obtain a better force-field, improving from the previous obtained force-field. Afterwards, the machine learning force-field is ready for the production run.[42–44]

Simulations Models

A single-layer pristine γ-graphdiyne is assumed to be planar and belongs to the *p6 m* two-dimensional space group.[45] Serafini et al developed an approach to generate and classify all possible GDY 2D structures.[46] A total of 26 structures were generated, including the polymorphs α-, β-, δ-, and γ-GDY. The γ-GDY (the common GDY) has gathered more attention in recent years, also from the experimental point of view. Among all the structures of this trend, γ- has the lowest energy compared to graphene, consistently with its low sp/sp^2 ratio.[46] The GDY unit cell is modeled by a (2×2) monolayer supercell containing 72 carbon atoms. Periodic boundary conditions are applied to simulate the infinite graphdiyne plane, as shown in Figure 1. For notation, we let the x and y directions be parallel and the z direction perpendicular to the single-layer GDY. To avoid interlayer interactions between image structures due to periodic calculations, a vacuum layer of 15 Å is set in the direction perpendicular to the monolayer GDY and it is optimized.

As an initial condition, all bond lengths are considered equal. Afterwards, all atomic positions and lattice constants are optimized by minimizing total energy and forces. In pristine GDY, the distance between the centers of two hexagons is equal to the lattice length a = 9.462 Å (a = b), which is in good agreement with the literature,[25,47] and the angle between them is γ = 120°. The bonds between hexagons are acetylenic linkages (–C≡C–) and the angle between them is γ = 180°. In this structure, four different carbon-carbon bond distances are present: the C=C bond in the benzene ring (d_A), the C–C (d_s) bond, the C≡C bond (d_T), and the C–C bond between two sp carbon atoms (d_{s1}) in diacetylenic linkages. These distances are indicated in Figure 1(a), and their values are listed in Table 1. The obtained values are respectively: 1.431 Å, 1.394 Å, 1.232 Å and 1.336 Å for pristine GDY, in good agreement with previously reported.[19] The cohesion energy is calculated according to Akbari et al.[36] and is −7.396 eV/atom, which is in good agreement with previously reported data.[47]

Firstly, we have investigated the most stable site for a single Li atom adsorption on graphdiyne monolayer. Different possible adsorption sites for the Li atom on GDY are tested: at the top of C atoms in the diacetylenic linkages (T1, T2 and T3), at bridge these linkages (B1, B2 and B3), at the center of triangular-like pores (H1), and at the center of the benzene ring (H2), as indicated in Figure 1(a).[48,49] The positive charged Li ion (Li^+) adsorption was also considered setting its initial state using the electrostatic corrections as implemented in VASP to localize the charge. However, all possible adsorption sites have positive adsorption energy values, indicating unstable systems. For this reason, our study focuses only on the neutral Li atom.

Next, to better understand the effect of defects on Li adsorption, we modeled a C vacancy in the GDY monolayer. For this, we removed one C atom at a time. The C atoms are labeled in Figure S1(a). The C–C bond distances and the vacancy formation energy (E_{form}) values are presented in Table S1 of the Supplementary Information (SI). It can be seen that all defective systems have similar E_{form} and generate almost the same bond distortion. Then, we only considered the defective system with the best formation energy for Li adsorption in the most stable configuration. Also, in Figure 1(b), it can be noted that new double C–C bonds labeled d_D are formed. The C vacancy introduces changes in the system's polarity, compared to perfect GDY. The charge distribution is symmetric in perfect GDY, with the benzene rings being more positive and mostly all Cs atoms forming the connective chains being negative (see Figure 2a). Removing one C atom leads to a redistribution of charge on the GDY layer with almost all C atoms closer to benzene rings being positive, while the rest of the

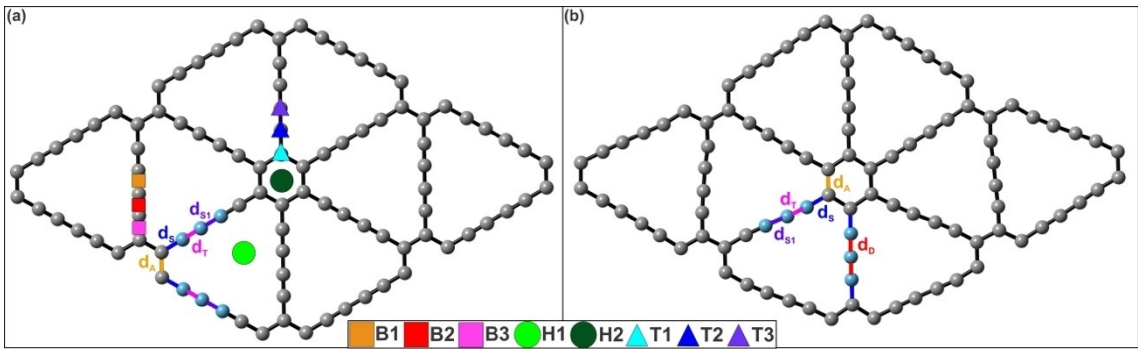

Figure 1. Schematic top view of two-dimensional GDY geometry structure of perfect (a) and defective (b) GDY. Adsorption sites and name bond distances are denoted. Carbon atoms are indicated with grey spheres.

Research Article
doi.org/10.1002/batt.202400514
Chemistry Europe
European Chemical Societies Publishing

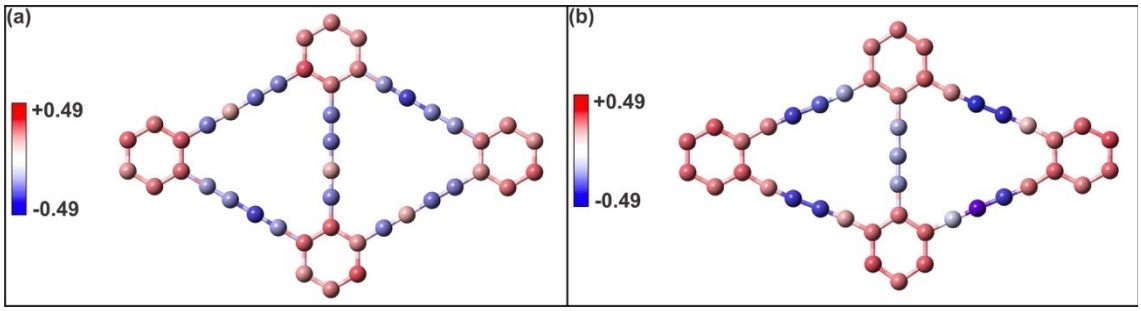

Figure 2. Charges among the C atoms of the perfect (a) and defective (b) GDY. Blue and red indicate the atom that gains (negative charge) and loses (positive charge) electrons, respectively. The bar on the left is in e^- unit.

connecting Cs are negatively charged. Also, the shortened arm shows a slightly decrease in the negative charge when compared with perfect GDY (see Figure 2b). A similar procedure for the analysis of charge distribution was applied by Houache et al [50].

We also study the capacity of perfect and defective GDY. For this, the considered adsorption sites in the plane are at the corners of the triangular-like pore. Then, one by one, the Li atoms are located at the corners of the triangular-like pore to form a triangle (see Figure S1 in SI).

2. Results and Discussion

2.1. Geometrical Properties, Energetic Analysis and Systems Stability

The bond distances and adsorption energies for all possible Li adsorption sites on perfect GDY are summarized in Table S2 in SI. It can be seen that, with the exception of the H2 site, all Li adsorbed configurations are energetically favorable, with the most favorable being the one corresponding to the H1 site.

Figure 3 shows the most stable adsorption configuration for perfect and defective GDY. In both cases, the Li is located at the corner of the triangular-like pore, but with a slight shift for the defective system. Table 1 presents the adsorption energy, C–C and C–Li bond distances for perfect and defective GDY before and after Li adsorption in the most stable configurations. The results show that the vacancy induces a distortion in the triangular-like pore and the formation of new C–C double bonds. Additionally, Li adsorption is more favorable in this system. In the perfect system, Li–C bonds are developed with distances ranging from 2.289 Å to 2.461 Å, while in the defective case these bonds are between 2.237 Å and 3.184 Å.

In Figures 4 and 5, AIMD simulations are depicted, which were performed to verify the stability of the Li adsorbed systems in its perfect and defective configuration.

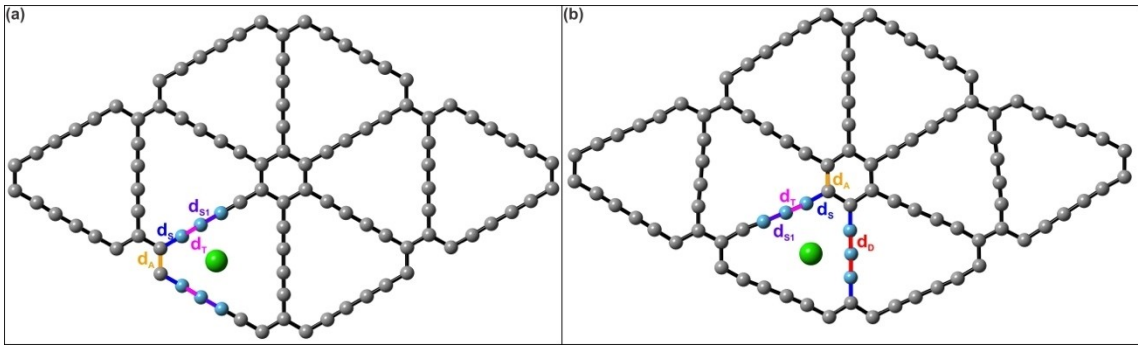

Figure 3. Schematic top view of two-dimensional GDY geometry structure for perfect (a) and defective (b) GDY after Li adsorption in the most stable configuration. Carbon and Lithium atoms are indicated with grey and green spheres, respectively.

Table 1. C–C, C–Li bond distances and E_{ads} for perfect and defective GDY before and after Li adsorption on the most stable systems. All bond distances are indicated in Figures 1 and 2.

System	d_A (Å)	d_s (Å)	d_T (Å)	d_{s1} (Å)	d_D (Å)	$d_{C\text{-}Li}$ (Å)	E_{ads} (eV)
Perfect	1.431	1.395	1.232	1.338	–	–	–
Li/Perfect	(1.428–1.431)	(1.394–1.400)	(1.233–1.239)	(1.338–1.342)	–	(2.289–2.461)	−2.521
Defective	(1.410–1.455)	(1.394–1.397)	(1.232–1.234)	(1.335–1.340)	(1.303–1.412)	–	–
Li/ Defective	(1.411–1.547)	(1.390–1.397)	(1.231–1.243)	(1.335–1.340)	(1.309–1.415)	(2.237–3.184)	−3.586

Research Article
doi.org/10.1002/batt.202400514
Chemistry Europe
European Chemical Societies Publishing

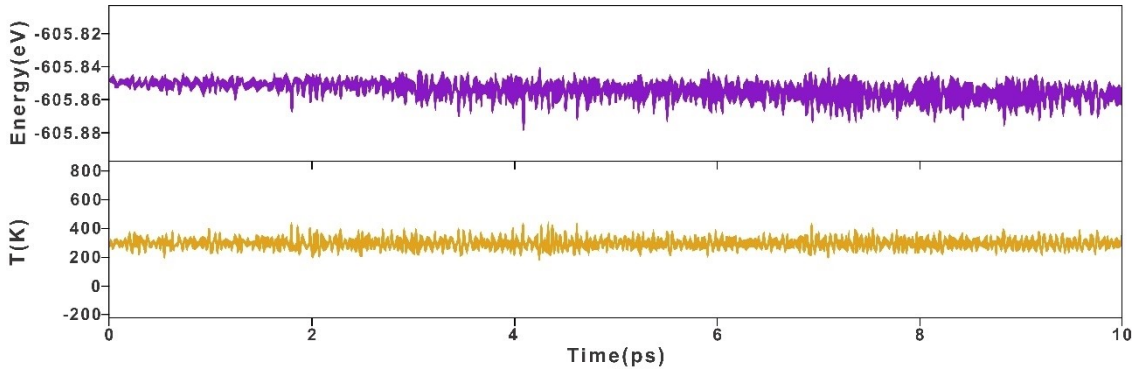

Figure 4. MLFF-AIMD simulations of total energy/ temperature evolution over time are presented for perfect GDY after Li adsorption in the most stable configuration. The step is 1 fs.

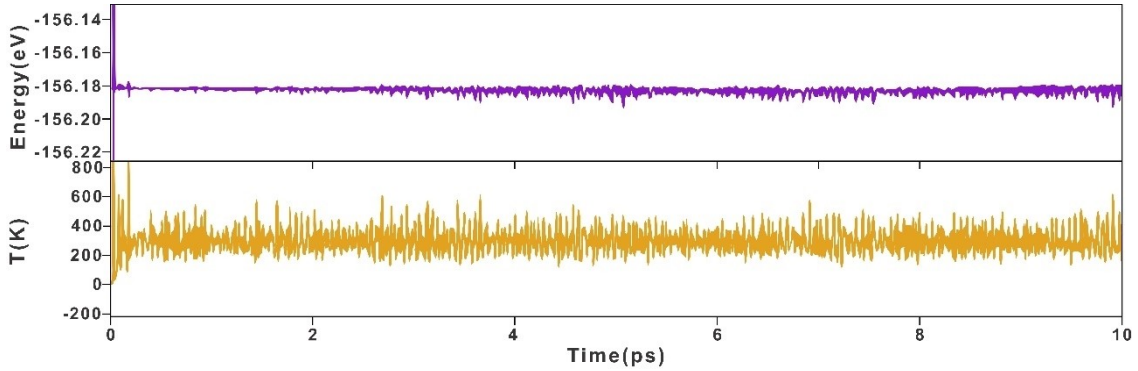

Figure 5. MLFF-AIMD simulations of total energy/ temperature evolution over time are presented for defective GDY after Li adsorption in the most stable configuration. The step is 1 fs.

The MLFF-AIMD simulations were performed in an NVT ensemble, with a Nosé-Hoover thermostat to control the temperature.[51] The simulations at 300 K were obtained with a time step of 1 fs, for a total time of 10 ps. It can be appreciated the insignificance of the energy and temperature variations, which confirms the stability of both systems.

2.2. Electronic Structure and Charge Analysis

Regarding the electronic structure, Figure 6 shows the total (a, b) and projected DOS (c,d) for the perfect and defective GDY before and after Li adsorption. The total DOS of GDY before adsorption presents a band gap of 0.46 eV. This semiconductor behavior is similar to the previous reports of Mohajeri and Shahsavar[52] and Li et al.[53]

In the perfect case, after Li adsorption the GDY–Li system becomes metallic and the Li 2 s states are stabilized (compare the green tick marks before adsorption and the green bands after adsorption, Figure 6a and c). C-based peaks in the region (0, −2) eV are shifted to lower energies after Li adsorption. This also happens in the region of (−4.3, −5) eV, and there is also a shift to lower energies below −5 eV. The C-atoms DOS intensity also decreases after Li adsorption. Considering the defective case, the vacancy makes GDY metallic, and after Li adsorption it shows an almost zero band gap. Lithium states become stabilized in the region (−1, −2) eV. There is also a decrease in the C-atom DOS intensity after adsorption. Li peak intensity shows higher hybridization when adsorbed on defective GDY.

The Bader charge analysis and charge density difference plots for the adsorption of Li at the most stable site of perfect and defective GDY are shown in Figure 7.

It can be seen that in both cases Li exhibits cationic behavior with a final charge of approximately +0.9e-. The C atoms closest to the adsorption site have a negative charge value ranging from −0.01e- to −0.30e- (−0.10e- and −0.35e−) for perfect (defective) GDY (Figure 7a and c). The plus and minus signs in the Bader charge indicate the loss or gain of electronic charge.

The charge transfer occurs near the vicinity of the Li atom adsorption site, with the Li atom transferring charge to the surface. The presence of a C vacancy results in the formation of new C–C bonds similar to double bonds, then a strong conjugation is enhancing the interaction with Li.

2.3. Bonding Analysis

The bond orders (BO) of C–C bonds and the sum of bond orders (SBO) for the C atoms in γ-GDY and GDY with a carbon vacancy (GDY defective) were studied considering the triangular array in Figure 1, where the bonds are indicated.

Research Article
doi.org/10.1002/batt.202400514
Chemistry Europe
European Chemical Societies Publishing

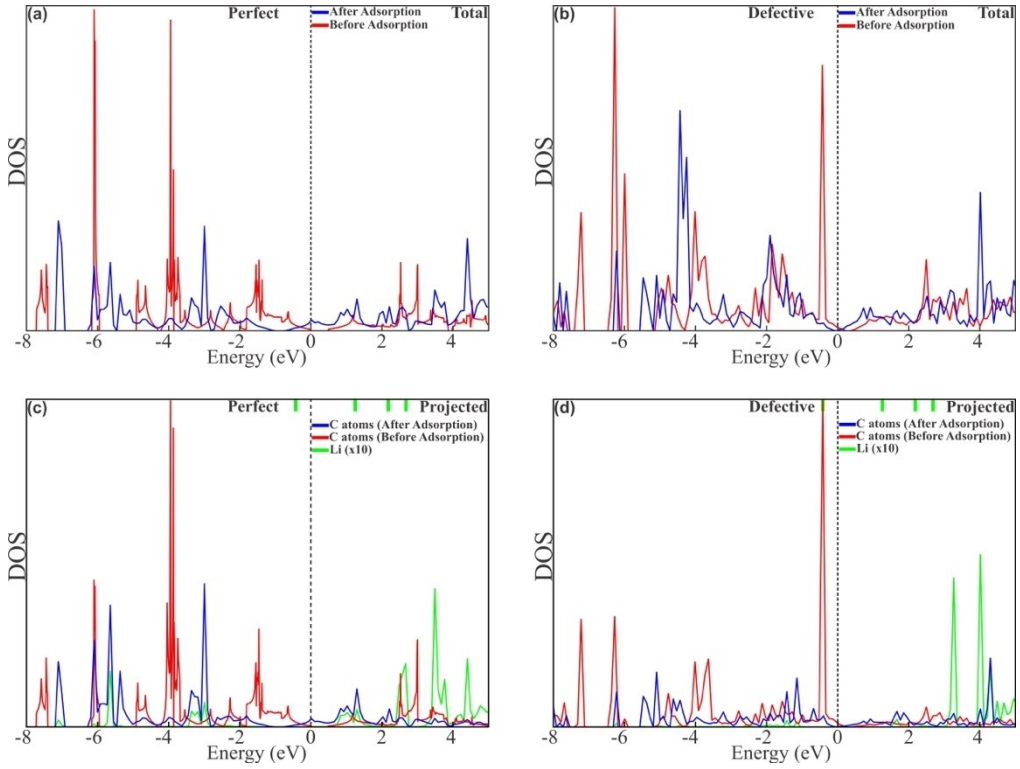

Figure 6. Total and projected DOS curves for perfect (a, c) and defective (b, d) GDY. The red and blue lines indicate the systems before and after adsorption. The green tick marks represent the positions of peaks for Li in vacuum.

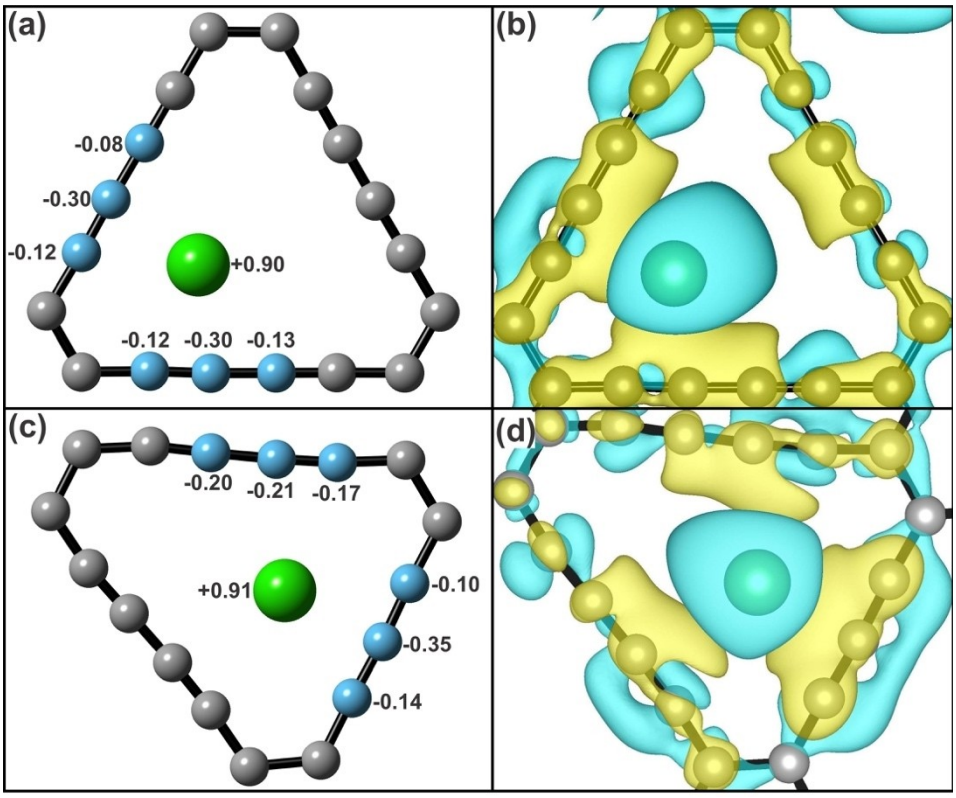

Figure 7. Schematic view of the environment of the most favorable Li adsorption site, with the Bader charge for the closest Li–C distances and top view of the charge density difference for perfect (a, b) and defective (c, d) GDY. The yellow and light blue regions indicate electron gain and loss of charge, respectively. The level of the isosurface is 0.0009 e / Å^3.

The BO of C–C bonds in the perfect arm of defective GDY shows minimal changes compared to γ-GDY. The single C–C BOs decrease slightly from 1.414 to 1.396 (d_s bonds, see Figure 1(a)) and from 1.821 to 1.804 (d_{s1} bond, see Figure 1(a)). This agrees with the slight expansion of the bond distance due to the vacancy presence. C–C triple bond BO (d_T) increases from 2.370 to 2.385 in agreement to bond shortening. Aromatic bonds near the vacancy do not present change, while those for the ring further away show a 1.1% BO increase. In the defective arm, the three remaining C atoms have formed double bonds (d_D) with BO between 2.056 and 2.206 (see Figure 1(b)). Single bonds between the aromatic ring and the defective arm show a BO decrease of around 1.5% in comparison to the perfect structure, corresponding to bond elongation.

The SBO for C atoms of the aromatic ring near the vacancy is about −1.0% lower than in the perfect structure, while for the atoms in the opposite ring increase by 0.7%. The C atoms in the defective arm of the triangular array presents a different behavior. The middle C atom's SBO increases from 4.293 to 4.354, while the other two decrease. The atom above the middle C atom changes from 4.293 to 3.688 (−14.0%) and the atom below the middle C of the arm changes from 4.059 to 3.830 (−5.6%), see Figure 1(b).

After Li adsorption, the BO of aromatic C–C bonds in γ-GDY weakens by about −1.7%. Single bond BO changes from 1.412 to 1.486 (d_s) and from 1.816 to 1.957 (d_{s1}) with a 7.8% change, while triple bond BO (d_T) increases from 2.378 to 2.396 (see Figure 1(a)). The Li–C bond BO ranges from 0.021 to 0.075, with distances ranging from 2.725 Å to 2.221 Å, respectively. In defective GDY + Li, the two double C–C bond BO in the short arm ranges from 2.166 to 2.184 (see Figure 1(b)), while single bonds between a C atom of the aromatic ring and a C from the defective arm decrease by −2.0%, in comparison to the perfect structure. The BO of the C–C aromatic bonds from the ring further away to the Li atom shows an increase of about 0.7%. Li–C bonds range from 0.010 to 0.090, with distances ranging from 3.180 Å to 2.244 Å, respectively.

All the C atoms SBO increase in both structures after Li adsorption. In the γ-GDY, that increment ranges from 0.7% to 5.5%, with the largest (smallest) change in C atoms forming single bonds in the middle in the arms of the triangular array (single bonded C atoms connected to the aromatic ring), being from 4.296 to 4.534 (4.065 to 4.093). In the case of the C atoms from the aromatic ring, the change is from 4.089 to 4.153. The SBO of the Li atom is 0.308. Meanwhile, in defective GDY, the SBO of C atoms increases between 0.4% and 6.0%, with the largest changes near the vacancy of C atoms closer to the Li atom (from 4.354 to 4.532). The other two C atoms of the defective arm change from 3.688 to 3.908 (second closest to Li atom) and from 3.830 to 3.920 (third closest to Li atom). The SBO of the Li atom is 0.317.

To summarize, the BO increase (decrease) corresponds to the shortest (largest) bond. A similar behavior was shown when we analyzed the bond orbital population (OP). There are no relevant general differences of the BO and SBO analysis between the pure and defective systems. However, it is relevant to mention that after Li adsorption, the SBO of all of the C atoms increases in both structures, showing a greater bond strength. This is in the same trend as the favorable adsorption energies in Table 1, which indicates that this system is more stable after adsorption, giving further support for considering this material for the implementation for energy purposes.

2.4. Theoretical Capacity and OCV

To study the GDY capacity, the number of Li atoms is increased one by one to fill the pores with the Li atom forming a triangular pattern, resulting in two possible stable configurations. One configuration has all the Li located on one side of the plane, while the other has Li atoms positioned above pores shoulder-by-shoulder but alternately on opposite sides of the graphdiyne layer (see Figure S1). The second configuration is the most stable and the GDY surface preserves perfectly flat, which is a necessary condition for the multilayered system. The maximum Li storage capacity achieved on perfect GDY is LiC_3, which is twice the capacity of graphite and agrees with the literature.[25,53,54] A higher concentration of Li atoms induces an important geometrical distortion which leads to structural collapse of the GDY layer. As a result, the maximum number of Li concentration is six. These distortions can be seen of the changes on the angles, which are consistent with a significant ripple in the layer (see Table S3 in SI).

For Li adsorption on this material, the maximum specific capacity obtained is 744 $mAhg^{-1}$, which agrees with that reported by Jang et al.[55] This capacity value is higher than the one for graphite (372 $mAhg^{-1}$),[56] which means that GDY is advantageous. Considering the high mobility and the high Li storage capacity, GDY can serve as a promising LiBs anode.

In Figure 8, the OCV values for the different concentrations of Li atoms adsorbed on the systems are shown.

When the atom concentration increases, the OCV values for Li decrease from 0.93 V to 0.23 V. The range is similar to the values obtained for B-graphyne by Yan et al. (0.2–1.2 V).[57] These OCV values are favorable because, in order to achieve the maximum voltage, the OCV of the anode with respect to Li metal needs to be low in LiBs when a cathode is present. The OCV profile should remain flat during lithiation to ensure good performance.[58]

For the defective GDY the maximum Li atom concentration configuration and number are the same as in the perfect case, which is reasonable because the vacancy only induces a shortening in a pore arm. For this system the specific capacity obtained is 788 $mAhg^{-1}$, which is slightly higher than for pristine GDY. In Figure 9, the OCV values for the different concentrations of Li atoms adsorbed on the defective system are shown.

In this case, when the atom concentration increases, the OCV values decrease from 0.48 V to 0.10 V, which is a lower range than for the pure case. Again, the OCV values obtained are favorable for medical applications and some display technologies such as pacemakers, sensors and e-paper, since they work with low voltage values.[59]

Research Article
doi.org/10.1002/batt.202400514
Chemistry Europe
European Chemical Societies Publishing

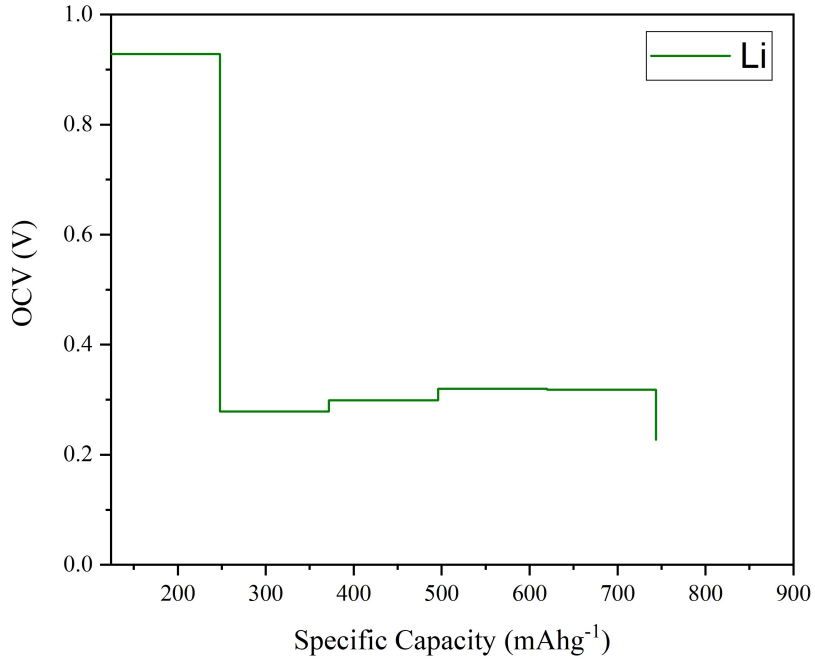

Figure 8. OCV vs Specific Capacity for GDY for different concentrations of Li (dark green curve).

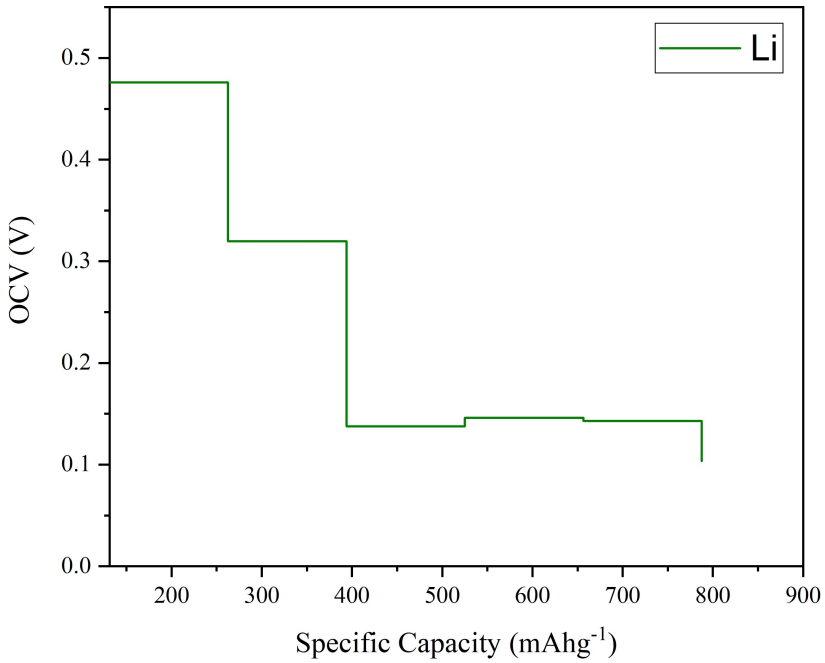

Figure 9. OCV vs Specific Capacity for defective GDY for different concentrations of Li (dark green curve).

3. Conclusions

We performed DFT calculations for pristine and defective GDY. We studied the effect of Li atoms adsorption on the electronic and structural properties of this 2D material. AIMD simulations show that both systems are stable. We analyzed different possible adsorption sites for the Li atom on GDY: at top C atoms in the diacetylenic linkages (T1, T2 and T3), at bridge sites (B1, B2 and B3), at the center of triangular-like pores (H1), and at the center of the benzene ring (H2). In both cases, the Li is located at the corner of the triangular-like pore, with a slight shift for the defective system. In the perfect system, Li–C bonds are developed with distances ranging from 2.289 Å to 2.461 Å, while in the defective case these bonds are between 2.237 Å and 3.184 Å. In the perfect case, the GDY–Li system becomes metallic and the Li 2 s states are stabilized. The vacancy makes GDY metallic, and after Li adsorption it shows an almost zero band gap. Lithium states become stabilized in the region (−1,

−2) eV. The charge transfer occurs near the vicinity of the Li atom adsorption site, with the Li atom transferring charge to the surface. The presence of a C vacancy results in the formation of new C=C bonds similar to double bonds, then a strong conjugation enhances the interaction with Li. After Li adsorption, the sum of all the C atoms sum of bond order increases in both structures, in the range 0.4% and 6%. The maximum Li storage capacity without significant restructuring is six Li atoms in both systems. When the atom concentration increases, the OCV values for Li decrease from 0.93 V to 0.23 V. In the case of defective GDY, the specific capacity obtained is 788 $mAhg^{-1}$, which is slightly above than for pristine GDY (744 $mAhg^{-1}$). These capacity values are higher than the one for graphite (372 $mAhg^{-1}$), which means that GDY is advantageous. Considering the high stability and the high Li storage capacity, GDY can serve as a promising LiBs anode.

Acknowledgements

Our work was supported by ANPCyT through PICT 2022 N° 2022–09–00775 and N° 2022–02–00049, PICT 2021 N° 2021-I-A-01144, PICT 2019 03491, PIP-CONICET 2021–2023 code: 11220200100944CO and PIP-CONICET 2021–2023 code: 11220200100941CO, PGI number 24/F083 research grants, as well as by SGCyT-UNS. AJ, EAG, PVJ, PB, MS, MJJ are members of IFISUR-CONICET. JJ is a fellow researcher at INFAP-CONICET.

Conflict of Interests

The authors declare no conflict of interest.

Data Availability Statement

The data that support the findings of this study are available from the corresponding author upon reasonable request.

Keywords: Graphdiyne · Lithium · Theoretical capacity · OCV · Electronic structures

[1] W. Chen, J. Liang, Z. Yang, G. Li, *Energy Procedia* **2019**, *158*, 4363–4368, https://doi.org/10.1016/j.egypro.2019.01.783.
[2] B. J. Landi, M. J. Ganter, C. D. Cress, R. A. DiLeo, R. P. Raffaelle, *Energy Environ. Sci.* **2009**, *2*, 638–654, https://doi.org/10.1039/b904116h.
[3] C. Capasso, O. Veneri, *Appl. Energy.* **2014**, *136*, 921–930, https://doi.org/10.1016/j.apenergy.2014.04.013.
[4] Q. Zhang, C. Tang, W. Zhu, C. Cheng, *J. Phys. Chem. C.* **2018**, *122*, 22838–22848, https://doi.org/10.1021/acs.jpcc.8b05272.
[5] E. Stura, C. Nicolini, *Anal. Chim. Acta.* **2006**, *568*, 57–64, https://doi.org/10.1016/j.aca.2005.11.025.
[6] H. J. Hwang, J. Koo, M. Park, N. Park, Y. Kwon, H. Lee, *J. Phys. Chem. C.* **2013**, *117*, 6919–6923, https://doi.org/10.1021/jp3105198.
[7] H. Li, L. Shi, Q. Wang, L. Chen, X. Huang, *Solid State Ionics* **2002**, *148*, 247–258, https://doi.org/10.1016/S0167–2738(02)00061–9.
[8] N. Duhan, T. J. Dhilip Kumar, *Appl. Surf. Sci.* **2024**, *642*, 158553, https://doi.org/10.1016/j.apsusc.2023.158553.
[9] Q.-K. Q.-X. DuWu, Q.-X. Wu, H.-X. Wang, X.-J. Meng, Z.-K. Ji, S. Zhao, W.-W. Zhu, C. Liu, M. Ling, C.-D. Liang, *Int. J. Miner. Metall. Mater.* **2021**, *28*, 1603–1610, https://doi.org/10.1007/s12613–020–2247–1.
[10] H. Liu, X. Zhang, Y. Zhu, B. Cao, Q. Zhu, P. Zhang, B. Xu, F. Wu, R. Chen, *Nano-Micro Lett.* **2019**, *11*, 65, https://doi.org/10.1007/s40820–019–0296–7.
[11] Y. Chabre, D. Djurado, D. Djurado, M. Armand, N. Coustel, W. R. Romanow, J. P. McCauley, J. E. Fischer, A. B. Smith, N. Coustel, J. E. Fischer, J. P. McCauley, A. B. Smith, *J. Am. Chem. Soc.* **1992**, *114*, 764–76, https://doi.org/10.1021/ja00028a056.
[12] E. Frackowiak, F. Béguin, *Carbon* **2002**, *40*, 1775–1787, https://doi.org/10.1016/S0008–6223(02)00045–3.
[13] B. Gao, A. Kleinhammes, X. P. Tang, C. Bower, L. Fleming, Y. Wu, O. Zhou, *Chem. Phys. Lett.* **1999**, *307*, 153–157, https://doi.org/10.1016/S0009–2614(99)00486–8.
[14] R. E. Ambrusi, C. R. Luna, M. G. Sandoval, P. Bechthold, M. E. Pronsato, A. Juan, *Appl. Surf. Sci.* **2017**, *425*, 823–832, https://doi.org/10.1016/j.apsusc.2017.07.070.
[15] E. Yoo, J. Kim, E. Hosono, H. Zhou, T. Kudo, *Nano Lett.* **2008**, *8*, 2277–2282, https://doi.org/10.1021/nl800957b.
[16] J. Hou, Y. Shao, M. W. Ellis, R. B. Moore, B. Yi, *Phys. Chem. Chem. Phys.* **2011**, *13*, 15384–15402, https://doi.org/10.1039/c1cp21915d.
[17] Z.-S. Wu, W. Ren, L. Xu, F. Li, H.-M. Cheng, *ACS Nano* **2011**, *5*, 5463–5471, https://doi.org/10.1021/nn2006249.
[18] K. T. Chan, J. B. Neaton, M. L. Cohen, *Phys. Rev. B: Condens. Matter Mater. Phys.* **2008**, *77*, 1–12, https://doi.org/10.1103/PhysRevB.77.235430.
[19] J. R. Dahn, *Phys. Rev. B.* **1991**, *44*, 9170–9177, https://doi.org/https://doi.org/10.1103/PhysRevB.44.9170.
[20] J. He, N. Wang, Z. Cui, H. Du, L. Fu, C. Huang, Z. Yang, X. Shen, Y. Yi, Z. Tu, Y. Li, *Nat. Commun.* **2017**, *8*, 1–11, https://doi.org/10.1038/s41467–017–01202–2.
[21] S. Rana, A. Kumar, P. Dhiman, G. Sharma, J. Amirian, F. J. Stadler, *Fuel.* **2024**, *356*, 129630, https://doi.org/10.1016/j.fuel.2023.129630.
[22] G. Li, Y. Li, H. Liu, Y. Guo, Y. Li, D. Zhu, *Chem. Commun.* **2010**, *46*, 3256–3258, https://doi.org/10.1039/b922733d.
[23] X. Gao, J. Li, R. Du, J. Zhou, M. Y. Huang, R. Liu, J. Li, Z. Xie, L. Z. Wu, Z. Liu, J. Zhang, *Adv. Mater.* **2017**, *29*, https://doi.org/10.1002/adma.201605308.
[24] H. Bao, L. Wang, C. Li, J. Luo, *ACS Appl. Mater. Interfaces.* **2019**, *11*, 2717–2729, https://doi.org/10.1021/acsami.8b05051.
[25] H. Zhang, Y. Xia, H. Bu, X. Wang, M. Zhang, Y. Luo, M. Zhao, *J. Appl. Phys.* **2013**, *113*, 1–5, https://doi.org/10.1063/1.4789635.
[26] G. Luo, X. Qian, H. Liu, R. Qin, J. Zhou, L. Li, Z. Gao, E. Wang, W. N. Mei, J. Lu, Y. Li, S. Nagase, *Phys. Rev. B: Condens. Matter Mater. Phys.* **2011**, *84*, 1–5, https://doi.org/10.1103/PhysRevB.84.075439.
[27] S. W. Cranford, M. J. Buehler, *Nanoscale* **2012**, *4*, 4587–4593, https://doi.org/10.1039/c2nr30921a.
[28] G. Kresse, J. Hafner, *Phys. Rev. B.* **1993**, *47*, 558–561, https://doi.org/10.1103/PhysRevB.47.558.
[29] G. Kresse, J. Hafner, *Phys. Rev. B.* **1993**, *48*, 13115–13118, https://doi.org/10.1103/PhysRevB.48.13115.
[30] G. Kresse, J. Furthmüller, J. Hafner, *Phys. Rev. B.* **1994**, *49*, 14251–14269, https://doi.org/10.1016/0927–0256(96)00008–0.
[31] P. E. Blöchl, *Phys. Rev. B.* **1994**, *50*, 17953–17979, https://doi.org/10.1103/PhysRevB.50.17953.
[32] J. P. Perdew, K. Burke, M. Ernzerhof, *Phys. Rev. Lett.* **1996**, *77*, 3865–3868, https://doi.org/10.1103/PhysRevLett.77.3865.
[33] H. J. Monkhorst, J. D. Pack, *Phys. Rev. B.* **1976**, *13*, 5188–5192, https://doi.org/10.1039/c8ta11250a.
[34] S. Grimme, J. Antony, S. Ehrlich, H. Krieg, *J. Chem. Phys.* **2010**, *132*, https://doi.org/10.1063/1.3382344.
[35] C. Sun, D. J. Searles, *J. Phys. Chem. C.* **2012**, *116*, 26222–26226, https://doi.org/10.1021/jp309638z.
[36] F. Akbari, A. Reisi-Vanani, M. H. Darvishnejad, *Appl. Surf. Sci.* **2019**, *488*, 600–610, https://doi.org/10.1016/j.apsusc.2019.05.272.
[37] E. Abduryim, C. Chen, L. Gao, S. Guo, S. Wang, Z. Zhang, Y. Cai, S. Gao, W. Chen, X. Guan, Y. Liu, G. Liu, P. Lu, *J. Phys. Chem. C.* **2024**, *128*, 6233–6248, https://doi.org/10.1021/acs.jpcc.4c00557.
[38] L. Shi, T. S. Zhao, A. Xu, J. B. Xu, *J. Mater. Chem. A.* **2016**, *4*, 16377–16382, https://doi.org/10.1039/C6TA06976B.
[39] Y. X. Yu, *Appl. Surf. Sci.* **2021**, *546*, 149062, https://doi.org/10.1016/j.apsusc.2021.149062.
[40] R. F. W. Bader, *Acc. Chem. Res.* **1985**, *18*, 9–15, https://doi. org/10.1021/ar00109a003..

[41] W. Tang, E. Sanville, G. Henkelman, *J. Phys. Condens. Matter* **2009**, *21*, https://doi.org/10.1088/0953–8984/21/8/084204.
[42] R. Jinnouchi, J. Lahnsteiner, F. Karsai, G. Kresse, M. Bokdaml, *Phys. Rev. Lett.* **2019**, *122*, 225701, https://doi.org/10.1103/PhysRevLett.122.225701.
[43] R. Jinnouchi, F. Karsai, G. Kresse, *Phys. Rev. B* **2019**, *100*, 014105, https://doi.org/10.1103/PhysRevB.100.014105.
[44] R. Jinnouchi, F. Karsai, C. Verdi, R. Asahi, G. Kresse, *J. Chem. Phys.* **2020**, *152*, 234102, https://doi.org/10.1063/5.0009491.
[45] R. H. Baughman, H. Eckhardt, M. Kertesz, *J. Chem. Phys.* **1987**, *87*, 6687–6699, https://doi.org/10.1063/1.453405.
[46] P. Serafini, A. Milani, D. M. Proserpio, C. S. Casari, *J. Phys. Chem. C* **2021**, *125*, 18456–18466, https://doi.org/10.1021/acs.jpcc.1c04238.
[47] N. Narita, S. Nagai, *Phys. Rev. B: Condens. Matter Mater. Phys.* **1998**, *58*, 11009–11014, https://doi.org/10.1103/PhysRevB.58.11009.
[48] T. He, S. K. Matta, G. Will, A. Du, *Small Methods* **2019**, *3*, 1–7, https://doi.org/10.1002/smtd.201800419.
[49] X. Qian, Y. Zheng, S. Chen, J. Xu, *Catalysts* **2020**, *10*, https://doi.org/10.3390/catal10080929.
[50] M. S. E. Houache, A. Shubair, M. G. Sandoval, R. Safari, G. A. Botton, P. V. Jasen, E. A. González, E. A. Baranova, *J. Catal.* **2021**, *396*, 1–13, https://doi.org/10.1016/j.jcat.2021.02.008.
[51] S. Nosé, *J. Chem. Phys.* **1984**, *81*, 511–519, https://doi.org/10.1063/1.447334.
[52] A. Mohajeri, A. Shahsavar, *J. Mater. Sci.* **2017**, *52*, 5366–5379, https://doi.org/10.1007/s10853–017–0779–1.
[53] Y. Li, L. Xu, H. Liu, Y. Li, *Chem. Soc. Rev.* **2014**, *43*, 2572–2586, https://doi.org/10.1039/c3cs60388a.
[54] C. Huang, S. Zhang, H. Liu, Y. Li, G. Cui, Y. Li, *Nano Energy* **2015**, *11*, 481–489, https://doi.org/10.1016/j.nanoen.2014.11.036 2211–2855.
[55] H. Lee, B. Jang, J. Koo, M. Park, H. Lee, J. Nam, Y. Kwon, *Appl. Phys. Lett.* **2013**, *103*, 0–5, https://doi.org/10.1063/1.4850236.
[56] Y. Wang, Y. Li, *J. Mater. Chem. A.* **2020**, *8*, 4274–4282, https://doi.org/10.1039/C9TA11589G.
[57] Y.-T. Yan, Z.-G. Shao, C.-L. Wang, L. Yang, *Phys. Lett.* **2022**, *804*, 139897, https://doi.org/10.1016/j.cplett.2022.139897.
[58] J. B. Goodenough, Y. Kim, *Chem. Mater.* **2010**, *22*, 587–603, https://doi.org/10.1021/cm901452z.
[59] D. C. Bock, A. C. Marschilok, K. J. Takeuchi, *Electrochem. Acta* **2012**, *84*, 155–164, https://doi.org/10.1016/j.electacta.2012.03.057.

Manuscript received: July 30, 2024
Revised manuscript received: September 17, 2024
Accepted manuscript online: October 14, 2024
Version of record online: November 7, 2024